

Large-scale error-correction protocols using global operations in ion traps

Yannick Seis,¹ Joseph F. Goodwin,² Benjamin J. Brown,³ and Terry Rudolph²

¹*Niels Bohr Institute, Blegdamsvej 17, 2100 Copenhagen Ø, Denmark*

²*Quantum Optics and Laser Science, Blackett Laboratory, Imperial College London, London, SW7 2AZ*

³*Niels Bohr International Academy, Niels Bohr Institute, Blegdamsvej 17, 2100 Copenhagen Ø, Denmark*

(Dated: May 10, 2019)

The technical demands to perform quantum error correction are considerable. The task requires the preparation of a many-body entangled state, together with the ability to make parity measurements over subsets of the physical qubits of the system to detect errors. Here we propose two trapped-ion experiments to realise error-correcting codes of arbitrary size to defend a single encoded qubit from dephasing errors. Novel to both of our schemes, which are achievable using both Penning traps and Paul traps, is the use of a global entangling phase gate. We make use of this entangling operation to significantly reduce the experimental complexity of state preparation and syndrome measurements. We also show, in our second scheme, that storage times can be increased further by repeatedly teleporting the logical information between two codes supported by the same ionic crystal to learn information about the locations of errors. We estimate that a qubit encoded in such a crystal will remain a high fidelity state for a time that is an order of magnitude longer than a qubit written to a single confined ion.

I. INTRODUCTION

The realisation of quantum technologies will require the long-term maintenance of coherent quantum states. To this end we have recently seen impressive experimental results demonstrating small instances of quantum error correction using superconducting qubits [1–5] and ion traps [6, 7]. These experiments demonstrate the manipulation of complex many-qubit entangled states such that encoded quantum information can be recovered, even if some of the physical qubits are subject to errors.

The long-term goal of quantum error-correction is to construct codes of arbitrary size that are robust to all types of local quantum noise. This ability will enable us to store quantum states with arbitrarily high fidelity by increasing the size of the quantum error-correcting code, provided the noise acting on the system is sufficiently weak. The preparation and manipulation of states stored in these codes presents a significant challenge, since it requires a high level of control over the physical components of the codes. To facilitate large scale error correction, it is thus desirable to find simple approaches to realise codes that extend the coherence time of an encoded logical qubit beyond that of its constituent parts [8].

In this Manuscript we propose a simple experiment to extend the coherence time of an encoded qubit by realising a large error-correcting code written on a Coulomb crystal of trapped ions. Given that trapped ion qubits are considerably more vulnerable to dephasing noise than depolarization (spin-flip) noise, improvements in coherence time can be achieved by using a biased code that protects the encoded information exclusively against dephasing errors. We thus propose an experiment to realise a repetition code of arbitrary size that is sufficient to protect against the most commonly occurring errors. Novel to our proposal is that all the necessary entangling operations are performed globally. This greatly reduces the experimental complexity of the scheme, as single ion

addressability is only required for initialisation and measurement. This is of particular utility to Penning trap implementations, where large Coulomb crystal qubit registers can be conveniently produced but addressing single ions is more challenging due to the rotation of the crystal.

Our scheme builds upon earlier work [9] where it is shown that both the five-qubit repetition code, and the five-qubit code [10] can be encoded and read out in a Penning trap using only global operations. In Ref. [9] the rotational symmetry of the Penning trap to exhaustively search for global operations that realise the required unitaries. Such a method is limited, as the space over which we must search grows rapidly with the size of the code. Here we take a systematic approach to discovering global entangling operations by studying only the centre-of-mass (COM) vibrational mode of the Coulomb crystal. We find that this global operation is sufficient to realise a repetition code of arbitrary size. We also propose a method of reading out syndrome data with global operations. We achieve this by partitioning our ion trap into two separate codes and teleporting the quantum information between the codes. The teleportation measurement corrects errors on the physical qubits, up to a Pauli error on the logical qubit, heralded by the outcome of the measurement.

Given that our scheme only defends against dephasing errors, we cannot scale the repetition code arbitrarily as the effects of spin-flip errors become appreciable in large codes. However, as the spin-flip rate is many orders of magnitude smaller than the dephasing rate, correcting dephasing errors allows us to improve the storage time of the encoded qubit. Our proposal may thus be integrated into distributed quantum error-correction schemes [11–14] to extend the lifetime of encoded qubits further. Distributed schemes have been considered explicitly for trapped ions in Refs. [15, 16]. We also point out recent work [17] where biased codes such as those we study have been considered in schemes for universal

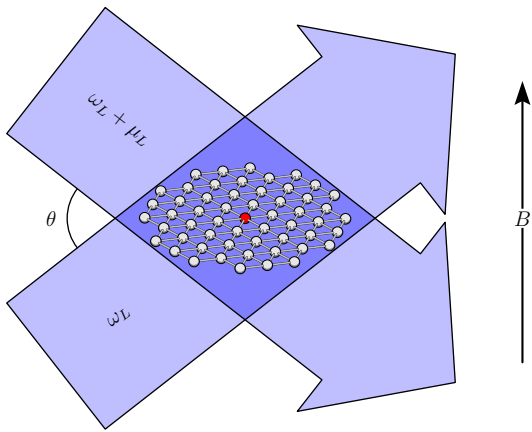


FIG. 1: A Penning trap with N ions and a static central ion coloured red. The optical dipole force beams shown in blue produce a travelling-wave optical lattice with wavevector perpendicular to the plane of the crystal. For appropriate choices of beam polarisation, this produces periodic, spin-dependent, optical dipole forces at the difference frequency μ_L .

quantum computation with low resource costs.

This Manuscript is structured as follows. In Sec. II we describe the experimental setup and the operations we require of our laboratory apparatus. In Sec. III we give the explicit programme to execute error correction. Finally in Sec. IV we consider the feasibility of our proposal by means of a noise analysis. We give some concluding remarks and propose further extensions of our work in Sec. V. Appendices A, B and C give technical details and important calculations.

II. EXPERIMENTAL SETUP

We consider a Coulomb crystal of N ions. Qubits are encoded on either the Zeeman or hyperfine sublevels of the $S_{1/2}$ ground state of each ion of the crystal, depending on the chosen species of ion. We will typically write qubits using the eigenbasis of the Pauli-Z operator, such that a qubit register is denoted $|\mathbf{s}\rangle = |s_1 s_2 \dots s_N\rangle$ where $s_j = 0, 1$. We denote the standard Pauli matrices acting on the j -th qubit of the register as X_j , Y_j and Z_j , and the eigenstates of the Pauli-X and Pauli-Y matrices are denoted $|\pm_x\rangle = (|0\rangle \pm |1\rangle)/\sqrt{2}$ and $|\pm_y\rangle = (|0\rangle \pm i|1\rangle)/\sqrt{2}$, respectively.

State preparation of the qubits is achieved by optically pumping the ions on a strong dipole transition, driving the population into $|0\rangle$ or $|1\rangle$ as required. Projective measurement in the Pauli-Z basis are performed by driving the qubit on the dipole transition and observing state dependent fluorescence. Collective local rotations $R_x(\theta)$ and $R_y(\theta)$ of all the qubits in the trap can be achieved via the application of radio-frequency (RF) or microwaves at the qubit splitting frequency.

Many-ion entanglement can be achieved via a gener-

alised geometric phase gate, namely a periodic, state-dependent optical dipole force (ODF) [9, 18, 19] tuned to a vibrational mode of the Coulomb crystal, entangling spin states to states of motion. If the ODF drive frequency is detuned from the vibrational resonance, the motional excitation will periodically return to zero. The spin states are thus disentangled from the motion having acquired a geometric phase proportional to the degree of excitation. [20, 21]

Such an ODF can be produced by a pair of crossed Raman lasers, as is depicted in Fig. 1, that produce a travelling one-dimensional optical lattice across the crystal with frequency μ_L , given by the frequency difference between the two laser beams. In general, the phase of the optical lattice must be the same for all the qubits driven by the entangling gate. For many-qubit gates this means that the plane of the lattice must be aligned to the plane of the Coulomb crystal, limiting us to driving transverse vibrational modes of one- and two-dimensional crystals. By tuning the ODF drive frequency to different vibrational modes of the crystal it is possible to achieve couplings to the qubit register identical to the mode geometry. Previously it was proposed to use such inhomogeneous couplings to produce complex entanglement in Penning traps, where the target state shared the symmetry of the driven mode [9]. However, the protocols described in this proposal can be achieved through excitations of COM mode only, which couples identically to all ions in the crystal, by driving at the normal mode frequency ω_1 .

A. Required operations for our error correction protocols

Using the setup described above, we design an experiment to prepare, maintain, and read out logical information encoded on a repetition code. For more details on repetition codes, we refer the reader to App. A. Here, we describe the operations that we require to follow the two different protocols given in Sec. III.

Both of our protocols require access to one single ion that we can prepare, measure, and rotate independently of the other ions of the crystal. This ion is used to address encoded information.

The remainder of the crystal must also be partitioned such that we can collectively initialise and measure all of the qubits of a given partition independently. More specifically, we have two protocols. In the simpler of the two, the remainder of the crystal need only form a single partition. In our second protocol where syndrome data can be continuously collected, we require the remaining ions of the crystal to be divided into two partitions.

Given a suitable partitioning, we can combine projective measurements and state preparation in the Pauli-Z basis together with collective RF or microwave rotations of the whole register. Given these operations it is possible to measure and prepare partitions in other bases as

required. As we only require control of the individual partitions during state preparation or readout, no local coherent control is required, avoiding the experimental complexity associated with high-fidelity single-qubit operations.

In general, addressing individual ions in a Penning trap is technically challenging as the crystal rotates at ~ 100 kHz. However we only need to independently address partitions of the crystal, not the individual ions within them, which can be more easily achieved if we partition the crystal into a series of concentric rings. A laser focused at the appropriate radial displacement will interact with each of the ions in a partition in turn, as the crystal rotation moves them through the beam. Fluorescence can be associated with each ion via time-tagging of the detected photons, a technique successfully demonstrated in a Penning trap [22]. Importantly, for an appropriate choice of N , the crystal will find an equilibrium configuration with a single ion that remains stationary at the centre of the rotating crystal. We refer to the central ion as the ‘hub’ qubit, shown in red in Fig. 2(a).

In a linear Paul trap, the partitions would be formed along a length of a one-dimensional Coulomb crystal, as shown in Fig. 2(b), while the single hub qubit could be any qubit in the string. State preparation and readout make use of individual addressing of the ions.

Both of our protocols also require the ability to perform a global entangling operation, namely

$$U = \prod_{j < k}^N CZ_{j,k}, \quad (1)$$

which applies the controlled phase gate, $CZ_{j,k} = (1 + Z_j + Z_k - Z_j Z_k)/2$, between all pairs of qubits in the crystal. Indeed, in App. B we show that driving the COM interaction for time $T = 2\pi k/\delta$, with integer k and detuning $\delta = \mu_L - \omega_1$, allows us to implement this unitary entangling operation up to single-qubit Pauli-Z rotations. Specifically, we have that $U \sim U'(T)$ where

$$U'(T) = e^{-iH_{\text{int}}T}, \quad (2)$$

with the interaction Hamiltonian for the COM vibrational mode

$$H_{\text{int}} = \frac{J}{N} \sum_{j < k}^N Z_j Z_k, \quad (3)$$

and

$$J \approx \frac{F^2}{4M\omega_1\delta}, \quad (4)$$

where each ion has mass M , and the travelling one-dimensional optical lattice imparts a periodic force on each ion with magnitude F .

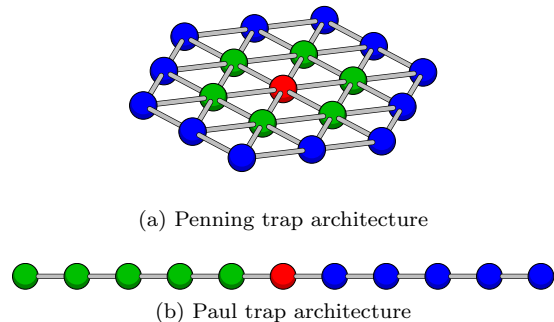


FIG. 2: The partition of our trapped ion crystal into two subsets (green and blue), with the hub qubit in the center (red).

III. PROTOCOLS

Having introduced the experimental setup we now give explicit programmes to carry out two different error-correction protocols, the *standard protocol*, and the *doubled protocol*.

The standard protocol encodes logical information onto one code of size $n = N - 1$ of the N ions in the crystal. This protocol only allows us to learn syndrome information when the encoded information is teleported back onto the hub qubit to be read out.

In the second protocol, the doubled protocol, we partition the crystal into two codes of size smaller than $N/2$. With this protocol, we are able to repeatedly obtain syndrome data by teleporting the encoded information between codes, thus enhancing our ability to correct for errors.

As the standard protocol is a special case of the doubled protocol, we give explicit details for the doubled protocol, and then summarise the simplification we make to execute the standard protocol.

A. The doubled protocol

We first define the code partitioning. The crystal is divided into three subsets \mathcal{Q}_1 , \mathcal{Q}_2 and \mathcal{Q}_h as is illustrated in Fig. 2. Subsets \mathcal{Q}_1 and \mathcal{Q}_2 support codes 1 and 2, respectively. As we have discussed above in Sec. II, our setup will only allow us to act on all of the members of a given subset uniformly. However we can collectively address all of the qubits of a given subset independently of all of the other subsets in order to initialise them and perform fluorescence measurements. The single element set \mathcal{Q}_h denotes the hub qubit which can be individually addressed.

In what follows we describe the steps to encode and read out quantum information from the qubit register, together with the steps we follow to learn syndrome data while information is encoded on the register. The following three steps first encode an arbitrary state onto qubit

subset \mathcal{Q}_1 .

1. Initialise the crystal such that the qubits of \mathcal{Q}_1 are in the state $|+x\rangle$, the qubits of \mathcal{Q}_2 in the state $|0\rangle$, and the hub qubit in the state we wish to encode $|\psi_y\rangle = \alpha|+y\rangle + \beta|-y\rangle$.
2. Apply the global unitary U .
3. Measure the hub qubit in the Pauli-X basis to teleport the information onto the crystal, up to a correction determined by the measurement outcome.

Having teleported the logical data onto a repetition code encoded on \mathcal{Q}_1 , we can now either learn syndrome data by teleporting the information onto \mathcal{Q}_2 , or we can read out the information by teleporting the logical state back to the hub qubit for readout. To read the information out, we proceed to step 7 below. To perform syndrome readout, we continue with steps 4 to 6.

4. Prepare all of the qubits of \mathcal{Q}_2 in the state $|+x\rangle$.
5. Apply the U operation
6. Measure all of the qubits of \mathcal{Q}_1 in the Pauli-X basis, and learn the majority measurement outcome which determines the correction we apply due to the teleportation operation.

In the programme between step 4 and step 6 we teleport information from code 1 to code 2 to obtain syndrome data. Analogously, if the information is stored on \mathcal{Q}_2 , we can also read out syndrome data by performing the reciprocal operation where we teleport the information from \mathcal{Q}_2 to \mathcal{Q}_1 .

We point out that, step 4 is achieved with several operations. We first pump all of the qubits in \mathcal{Q}_2 into the state $|0\rangle$. Then, we perform a collective local $R_y(\pi/2)$ rotation over the entire crystal using a microwave pulse. Importantly, the information encoded in \mathcal{Q}_1 is invariant under this rotation, see App. A.

It is also worth noting that while we carry out steps 4 through 6, the hub qubit remains idle. During this period, the experimentalist is free to include the hub qubit within one of the code subsets provided it is once again isolated before proceeding to step 7. Indeed, if we are satisfied with the partition \mathcal{Q}_1 containing only a single qubit, taking this liberty gives us the smallest realisations of our protocol. In particular, if we take $\mathcal{Q}_1 = \mathcal{Q}_h$ throughout steps 4, 5 and 6, we can perform an example of the doubled protocol using only four qubits in a Paul trap and six qubits in a Penning trap.

In the final steps we read quantum information out from the code, where in the following steps we suppose that information is stored on code 1. However, the steps are easily adapted if information is stored on code 2.

7. Initialise the hub qubit to $|+x\rangle$ and pump the qubits \mathcal{Q}_2 onto an eigenstate of the Pauli-Z operator.

8. Apply U .

9. Measure the qubits of \mathcal{Q}_1 in the Pauli-X basis and record to majority outcome to teleport logical information back to the hub and learn the appropriate Pauli correction.

With the logical information moved back to the hub qubit, we are free to extract this quantum information via single-qubit operations.

B. The standard protocol

In the standard protocol we follow the programme above, except steps 4, 5 and 6 are skipped. Moreover, qubit subset \mathcal{Q}_2 is an empty subset, and \mathcal{Q}_1 contains all of the qubits of the crystal except for the hub qubit.

IV. NOISE ANALYSIS

Here we investigate how our two proposals perform in a realistic laboratory environment to learn their experimental viability. The noise analysis we now present also allows us to compare the merits of our protocols, and to optimise their parameters.

A. Noise model

Qubits encoded in ions suffer dephasing errors much more rapidly than they suffer spin flips. To model this noise bias, we have that ions dephase with rate γ_Z , and spin flips occur at a rate γ_X . The *noise bias* is thus defined as $\eta = \gamma_Z/\gamma_X$. Unless we specify otherwise, we will always take $\eta \sim 10^4$, as this is a typical value for qubits encoded in electronic ground state sublevels. For convenience we will work in units where $\gamma_Z = 1$.

Given these parameters, the noise incident to each ion is described by the noise map $\mathcal{E} = \mathcal{E}_Z \circ \mathcal{E}_X$, where \mathcal{E}_X (\mathcal{E}_Z) describe spin-flip (dephasing) noise acting on each individual ion of the system. Specifically, we write these maps as

$$\mathcal{E}_\sigma(\rho) = (1 - p_\sigma(t))\rho/2 + p_\sigma(t)\sigma\rho\sigma/2, \quad (5)$$

where $\sigma = X, Z$ are the standard Pauli matrices,

$$p_X(t) = (1 - e^{-t/\eta})/2, \quad (6)$$

and

$$p_Z(t) = (1 - e^{-t})/2. \quad (7)$$

It is worth noting that the noise channels \mathcal{E}_Z and \mathcal{E}_X commute. We are therefore able to treat the two channels separately. To simplify our analysis, we also frequently make the assumption that $p_X(t)$ and $p_Z(t)$ are small.

B. Figure of merit

To quantify and compare the performance of different protocols, we require a suitable figure of merit. A quantum error-correcting code must maintain an encoded qubit at arbitrarily high fidelity for the duration of its designated task. We take our figure of merit to be the *high-fidelity time* as defined in Ref. [9]. Specifically, we calculate the time, τ , before which no logical error, of any form, has been introduced to the encoded information with probability more than $\epsilon \sim 0.01$. We make this definition more rigorous as it becomes required. Maximising this storage time for the parameters of the protocols will allow us to compare the storage schemes with information storage in a single qubit.

C. The standard protocol

We first consider the standard protocol using a crystal of N ions. We teleport information from the central hub ion onto a code of size $n = N - 1$. We then teleport the information back to the hub qubit to read the encoded information. We point out that this protocol is a generalisation of the repetition-code protocol presented in Ref. [9] where $N = 6$.

As we will show, we find that we can extend the storage time over that of a qubit encoded with a single ion by a factor of up to 77 for the case where $\eta \sim 10^4$. We achieve this improvement with a crystal of size increasing up to $N \sim 130$ ions, when X errors become limiting.

With the repetition code, the logical information is lost once a single spin flip is introduced to the system. We find the probability $\bar{P}_X(t, n)$ that a single spin has flipped scales linearly with n as described by the first-order expression

$$\bar{P}_X(t, n) \approx np_X(t) \approx \frac{nt}{2\eta}. \quad (8)$$

where each ion of the system is subject to the noise map \mathcal{E}_X given in Eqn. (5), and where we have assumed that $p_X(t)$ is small.

The repetition code we prepare can tolerate up to $(n - 1)/2$ dephasing errors. The probability that a majority of qubits suffer a dephasing error is

$$\bar{P}_Z(t, n) = \sum_{j=n_e}^n \binom{n}{j} p_z(t)^j (1 - p_z(t))^{n-j}, \quad (9)$$

where each ion is subject to the noise map \mathcal{E}_Z and $n_e = (n - 1)/2$ when n is odd and $n_e = n/2 - 1$ when n is even.

We optimise the performance of the code by choosing n such that the logical failure rate due to bit-flips and dephasing errors *both* remain suitably low. We thus seek to find $n = n_{\text{opt}}$ such that this is the case.

If the number of ions is too few, the logical information is vulnerable to phase-flips. At the same time, bit-flip errors degrade the stored state by a small amount.

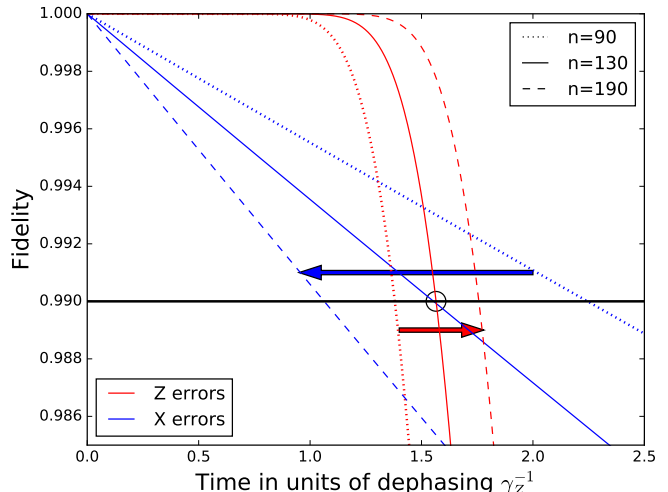


FIG. 3: The fidelity due to bit-flips (blue) and phase-flips (red) at a fixed ratio $\eta = 10^4$ for varying number of physical qubits: 90 (dotted), 130 (solid) and 190 (dashed). The resistance of the code to phase-flips improves with increasing number of qubits (red arrow), but its resistance to bit-flips decreases (blue arrow). The optimal number of physical qubits in the standard protocol for $\eta = 10^4$ is about 130, which is when the fidelity loss due to bit and phase-flips is the same. The maximum storage time is then $\tau_1 = 1.6 \cdot \gamma_Z^{-1}$.

By increasing n , we improve the protection that the code offers against dephasing errors. However, logical errors due to bit flips become more appreciable. If n becomes too large, while we have very good protection against dephasing errors, the probability that a logical error occurs due to bit-flip errors becomes too great.

We find the optimal number of ionic qubits, n_{opt} , such that the high fidelity time of the standard code protocol, τ_1 , is optimised. Specifically, we will evaluate n_{opt} such that

$$\bar{P}_Z(\tau_1, n_{\text{opt}}) = \bar{P}_X(\tau_1, n_{\text{opt}}) = \epsilon. \quad (10)$$

In Fig. 3 we illustrate the performance of the code for different values of n . As the number of qubits is increased towards n_{opt} , the logical X and Z error probabilities converge. The optimal case is indicated by the black circle in Fig. 3, where the solid red and blue curves intersect.

We now look to find the optimal number of ions for a range of noise bias η and at how to determine the improvements in high-fidelity time. In Fig. 4 we plot n_{opt} as a function of η where solutions of Eqn. (10) are evaluated numerically. We find that the optimal number of physical qubits in the code increases as a power law with η . Specifically, for our choice of $\epsilon = 0.01$, we find from the data that the optimal number of ions scales with η by the expression

$$n_{\text{opt}} = 0.0675 \cdot \eta^{0.815} + 5.5. \quad (11)$$

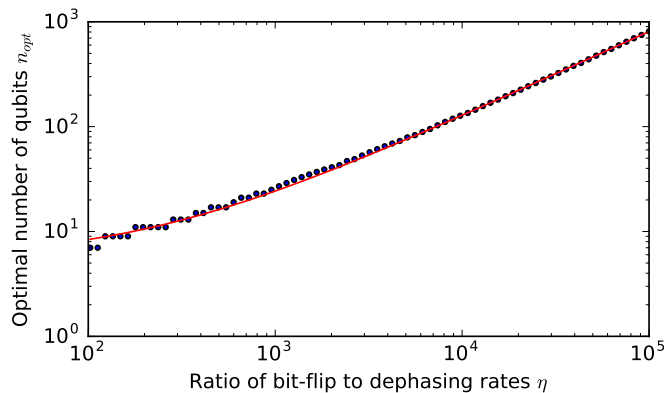


FIG. 4: The optimal number of qubits as function of qubit bias η . This is the qubit number for which the state fidelity is degraded by the same amount by X and Z errors. A fit $n_{\text{opt}} = 0.0675 \cdot \eta^{0.815} + 5.5$ is given by the red curve.

Having evaluated n_{opt} we can now determine the optimal high-fidelity time for a given species of ion with noise-bias value η . We substitute Eqn. (11) into Eqn. (10) using Eqn. (8) to find

$$\tau_1 = \epsilon\eta/n_{\text{opt}} \sim 14.8 \cdot \epsilon \cdot \eta^{0.185}. \quad (12)$$

From this expression, we have $\tau_1 = 1.6 \cdot \gamma_Z^{-1}$ by taking $\eta \sim 10^4$. We finally compare this time with the high-fidelity time τ_0 of a qubit encoded in a single ion subject only to Z errors. From Eqn. 7, we have

$$\tau_0 = -\log(1 - 2\epsilon) \sim 0.02 \cdot \gamma_Z^{-1}. \quad (13)$$

For the case, again, where $\eta = 10^4$, we find $\tau_1/\tau_0 \sim 77$ for a crystal of size $N = n_{\text{opt}} \sim 130$ ions. Hence a substantial improvement in storage time is achieved with this protocol.

Next, we will compare the doubled protocol with the standard protocol where we will take the standard protocol at its optimal size $n_{\text{opt}} \sim 130$ for the case where $\eta = 10^{-4}$.

D. The doubled protocol

This protocol allows us to read out syndrome information continuously while information is stored which enables us to identify and correct dephasing errors that are incident to the physical qubits of the code. This ability comes at the expense of reducing the number of encoded qubits of the crystal by more than half. However, we will show that we can extend the coherence time of encoded information beyond that of the standard protocol. This will come with the condition that we perform teleportations frequently enough such that logical information is repeatedly moved onto a new pure code state before too many errors accumulate.

Here, we compare the performance of this alternative scheme to that of the standard protocol where we consider variations in the teleportation frequency. For now, we take the simplified case where we assume that we can perform teleportation operations without introducing additional errors to the system.

We consider the explicit example of a crystal of reasonable size where $N \gtrsim 2n_{\text{two}} \sim 53$ with $\eta \sim 10^4$. The calculations to follow show that the doubled protocol of size $n_{\text{two}} \sim 26 = n_{\text{opt}}/5$ will outperform the standard protocol where $N \sim n_{\text{opt}} \sim 130$ provided we can teleport with frequency $K_{\text{min}} \sim 1.5 \cdot \gamma_Z$; a frequency we believe to be achievable using existing technology.

Further, given that the code used in the doubled protocol is a factor of 5 smaller than the crystal used in the standard protocol, we have also decreased the rate at which logical errors occur due to bit-flips. We may thus increase the teleportation frequency to extend the protection of the system against dephasing errors such that we reach the regime where bit flips again become the limiting factor. We find below that, if we can perform teleportations at a rate $K_{\text{max}} \sim 1.9 \cdot \gamma_Z$, the doubled protocol will exceed the coherence time of the standard protocol by a factor of 5. It is in fact in our interest to make the codes as small as possible in order to minimise bit-flips and maximise the high-fidelity time. The speed at which we can perform teleportations between codes will set a lower bound on the size of the code.

We now proceed with the calculation to find the above results. We first consider the noise the doubled protocol must tolerate. The doubled protocol will tolerate logical errors due to bit-flips at rate $\bar{P}_X(t, n_{\text{two}})$, as given by Eqn. 8.

As with the previous study of the standard protocol, we compare Eqn. (8) to the rate at which dephasing errors occur. Specifically, after teleporting the information between the codes at a frequency K and for a time t , the probability of logical failure due to dephasing is given by the expression

$$\bar{P}_{Z,tele}(t, K, n_{\text{two}}) = Kt \bar{P}_Z\left(\frac{1}{K}, n_{\text{two}}\right), \quad (14)$$

where the factor Kt gives the number of teleportations which we have performed over time t , and $1/K$ is the time interval between teleportations.

We define K_{min} to be the smallest teleportation frequency which allows us to outperform the standard code at time τ_1 , i.e., such that the dephasing fidelity of logical information in the doubled protocol is higher than $1 - \epsilon$ at τ_1 . To calculate K_{min} , we compare Eqn. (14) to Eqn. (8) (which by definition of n_{opt} is equal to Eqn. (9) at τ_1), then K_{min} is the smallest frequency for which

$$\bar{P}_{Z,tele}(\tau_1, K_{\text{min}}, n_{\text{two}}) < \bar{P}_X(\tau_1, n_{\text{opt}}) \quad (15)$$

In Fig. 5, we show how K_{min} may be found graphically for $n_{\text{two}} = 26$. We need to teleport before the dephasing fidelity of the doubled protocol (continuous blue

line) goes below the bit-flip fidelity of the standard code $1 - \bar{P}_X(t, n_{\text{opt}})$ (green dotted line). The latest time t_{min} at which this can be done is emphasised by the green circle. Teleporting at a frequency $K_{\text{min}} = 1/t_{\text{min}}$ keeps the dephasing fidelity of the doubled protocol (continuous green line) above the standard code bit-flip fidelity, and dephasing fidelity (dashed black line) at time τ_1 (black circle). For our specific case, we find $K_{\text{min}} = 1.5 \cdot \gamma_Z$.

We have thus shown we may outperform the standard protocol by teleporting the stored qubit between two codes of smaller size. However teleporting at frequency K_{min} only allows us to keep high fidelity up to time τ_1 . We now show how to calculate the teleportation frequency in order to keep high dephasing fidelity up to time τ_2 , when dephasing and bit-flip errors in the doubled protocol equate.

In an analogous manner, we thus define a teleportation frequency K_{max} , by comparing Eqn. (14) to Eqn. (8), as

$$\bar{P}_{Z,tele}(\tau_2, K_{\text{max}}, n_{\text{two}}) < \bar{P}_X(\tau_2, n_{\text{two}}). \quad (16)$$

Again Fig. 5 allows us to find the latest time t_{max} (red circle) by which we need to teleport in order to keep a high dephasing fidelity up to τ_2 . We find that teleporting at $K_{\text{max}} = 1/t_{\text{max}} = 1.9 \cdot \gamma_Z$ allows us to keep the dephasing fidelity above the bit-flip fidelity of the doubled protocol (red dotted line).

In general, we can improve the high-fidelity time of the crystal by decreasing the size of the code and increasing teleportation frequency. However, from a practical perspective, the rate at which we can perform high-fidelity teleportation operations is finite for a given experimental setup. It is thus interesting to learn how best to scale K as a function of decreasing n_{two} . In Fig. 6, we plot the teleportation frequencies K_{min} and K_{max} for varying code sizes n_{two} . We can now ask if one can experimentally teleport at a frequency K_{lab} , what are the best code sizes for the doubled protocol, n_{min} and n_{max} , such that we respectively outperform the standard code at τ_1 , and increase storage time to τ_2 .

For an explicit example we take a modest laboratory teleportation frequency $K_{\text{lab}} = 3 \cdot \gamma_Z$ (dotted black line in Fig. 6) and find that $n_{\text{min}} = 13$ is the smallest number of qubits for which $K_{\text{min}} \leq K_{\text{lab}}$. Similarly $n_{\text{max}} = 19$ gives $K_{\text{max}} \leq K_{\text{lab}}$.

We remark that changing n_{two} may influence how many teleportations can be made since typically entangling operations become more difficult the more qubits are involved. Therefore finding the best code size and number of teleportations may require some trial and error calculations.

We notice that $K_{\text{min}} \sim K_{\text{max}}$. We therefore aim to always teleport at frequency K_{max} in order to also maximise storage time.

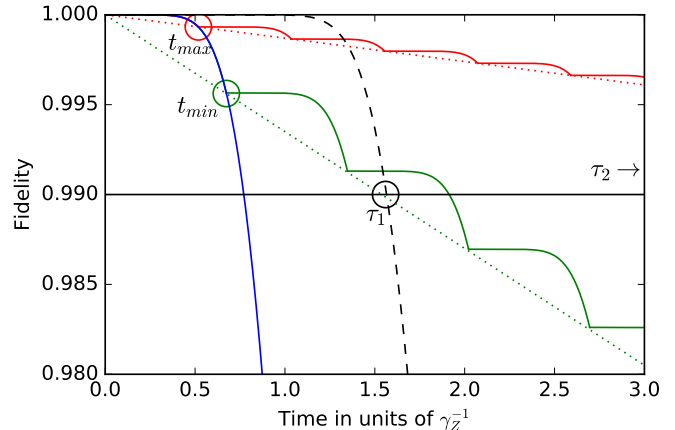


FIG. 5: Minimal and maximal teleportation frequency. The blue curve gives the fidelity $1 - \bar{P}_Z(t, n_{\text{two}})$ of a code of size n_{two} subject to Z-errors when no teleportations are performed. The fidelity due to X-errors for codes of size $n_{\text{opt}} = 130$ and $n_{\text{two}} = 26$ are given by the dotted green and red lines. To outperform the standard code, the first teleportation needs to occur at t_{min} , indicated by the green circle, and thereafter periodically teleport at a frequency $K_{\text{min}} = t_{\text{min}}^{-1} = 1.5 \cdot \gamma_Z$ such that the fidelity of the doubled protocol stays above the dotted green line. To maximise the potential of the doubled protocol, we must start teleporting earlier (at time t_{max} indicated by the red circle) and more frequently at frequency $K_{\text{max}} = t_{\text{max}}^{-1} = 1.9 \cdot \gamma_Z$ in order to stay above the fidelity due to X-errors (dotted red line).

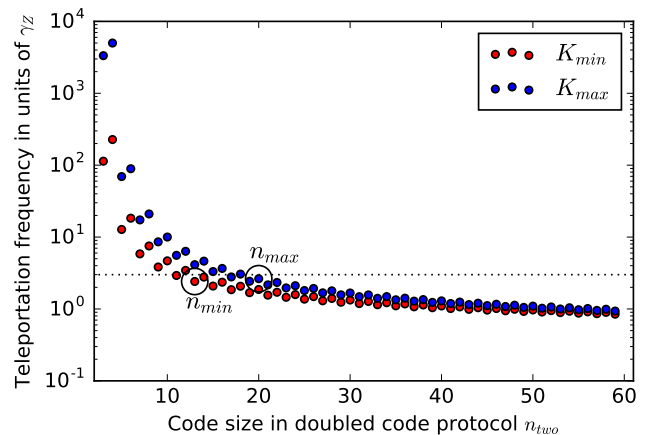


FIG. 6: Teleportation frequencies for varying code sizes. For two codes of size n_{two} , teleporting at a frequency of at least K_{min} will outperform the standard code with optimal qubit number in storage fidelity. Teleporting with frequency above K_{max} , maximises the storage time in the doubled protocol since the X-errors are limiting the storage fidelity. If we can experimentally perform teleportations at a frequency of, for example, $K_{\text{lab}} = 3 \cdot \gamma_Z$ (dotted black line), we can implement a good storage with the doubled protocol using $13 \leq n_{\text{two}} \leq 19$.

1. Imperfect teleportations

The discussion given so far has assumed we can perform teleportation operations without introducing any additional noise to the system. However, this is an unphysical assumption we have made to simplify calculations. Finally, we discuss errors that may occur during the teleportation operation.

Dephasing errors are induced by applying the entangling Hamiltonian incorrectly. This can include fluctuations in the laser intensity and deviations from the ideal interaction time T . Certainly, our code is designed to protect against dephasing errors. Therefore, these errors can be corrected in our code provided the entangling operation is performed with suitably high fidelity, with some cost in dephasing error rate the protocol can tolerate.

Spin-flip errors can be caused by spontaneous Raman scattering during the entanglement operation and the scattering of photons by neighbouring ions during the teleportation and readout phase. Spin-flip errors during the entangling evolution cannot be corrected and need to be kept low. We denote D to be the probability that one spin-flip error is introduced across the entire crystal when applying the teleportation operation. We take the error probability into account by rewriting Eqn. (8). We redefine the maximum storage time τ'_2 as

$$\frac{n_{\text{two}}\tau_2}{2\eta} = \epsilon \rightarrow \frac{n_{\text{two}}\tau'_2}{2\eta} + K\tau'_2 D = \epsilon \quad (17)$$

where the number of teleportations done during the storage protocol is $K\tau'_2$. Eqn. (17) is defined such that the term $n_{\text{two}}\tau'_2/2\eta$ accounts for the natural spin flips of our ions, and the term $K\tau'_2 D$ takes into account the bit-flips induced by the entangling and teleportation operations.

Indeed, the value of D is highly dependent on the underlying experimental architecture. We leave a full analysis of the errors that occur due to global entangling operations to future work.

V. CONCLUSION

To summarise, we have introduced two experiments to protect encoded quantum information using a trapped-ion architecture. Remarkably, our noise analysis shows that we can improve high-fidelity storage times by more than an order of magnitude for realistic ion trap setups, when compared with the storage time of a single qubit. We believe such protocols are achievable with standard ion trapping and manipulation techniques already widely in use in the community. It is noteworthy that the smallest instances of our proposals are realised with only four ions in a Paul trap and six ions in a Penning trap.

We expect that the protected qubits we propose could be integrated into a distributed scheme, where separate logical qubits are optically linked. Improvements in the

memory time of individual qubit nodes that our scheme can provide may improve the quantum resource cost of such systems. It will also be interesting to extend this work by discovering new schemes to realise other interesting codes, for instance codes which also protect against spin-flip errors. Such a proposal will require further analysis of the entangled states that can be realised with global entangling operations on large-scale Coulomb crystals. We leave these questions open for future work.

Acknowledgments

The authors would like to thank Chris Monroe for encouraging discussions and Anders Sørensen for his insights and outlook on our proposal, and for critiquing our Manuscript. YS is supported by ERC Grant Q-CEOM, BJB is supported by the Villum Foundation, JFG and TR are supported by the EPSRC.

Appendix A: The repetition code

In this Appendix we give explicit details on the repetition code. We describe how to teleport encoded quantum states between two separate repetition codes to learn the locations of incident dephasing errors using the global operation and single-qubit measurements described in Subsec. II A. We also show that we can encode arbitrary states to the repetition code using the same operations.

1. Codewords

The repetition code encodes one logical qubit in a subspace of n physical qubits. Encoded states, or *codewords*, of the code are spanned by the basis

$$|\bar{0}_y\rangle = \underbrace{|+_y\rangle |+_y\rangle \dots |+_y\rangle}_n, \quad (A1a)$$

$$|\bar{1}_y\rangle = \underbrace{|-_y\rangle |-_y\rangle \dots |-_y\rangle}_n, \quad (A1b)$$

where we remind the reader that $|\pm_y\rangle$ ($|\pm_x\rangle$) are eigenstates of the Pauli-Y (Pauli-X) operator. We follow the convention where we denote vectors in the logical basis with a bar above the vector label. We thus write a logical qubit encoded in an arbitrary state as

$$|\bar{\psi}_y\rangle = \alpha |\bar{0}_y\rangle + \beta |\bar{1}_y\rangle. \quad (A2)$$

It will also be convenient to define the codewords of the repetition code prepared in an alternative basis, $|\bar{0}_x\rangle$ and $|\bar{1}_x\rangle$, such that

$$|\bar{0}_x\rangle = \underbrace{|+_x\rangle |+_x\rangle \dots |+_x\rangle}_n, \quad (A3a)$$

$$|\bar{1}_x\rangle = \underbrace{|-_x\rangle |-_x\rangle \dots |-_x\rangle}_n. \quad (A3b)$$

Both of the encoding schemes defined in Eqns. (A1) and (A3) allow to detect dephasing errors. When a dephasing error affects a physical qubit in a Pauli- X or Pauli- Y eigenstate, it is flipped to the other eigenstate of the same basis.

This property will allow us to correct dephasing errors incident on the physical qubits. This correction is done when reading out the logical information, as described at the end of the next Subsection.

2. Syndrome readout by teleportation

We first show that we can use a global entangling operation together with single-qubit measurements to learn syndrome information. We begin with two codes prepared in the initial state

$$|C_0\rangle = |\bar{\psi}_y\rangle_1 |\bar{0}_x\rangle_2. \quad (\text{A4})$$

where the encoded information is stored on the first code, indexed 1, and we prepare a second code, indexed 2, in the logical state shown in Eqn. (A3a). Each code can take an arbitrary size and they do not necessarily have to use the same number of physical qubits.

We entangle the codes in Eqn. (A4) with a global entangling operation, U , given in Eqn. (1), to obtain the state

$$|C_1\rangle = U|C_0\rangle = |\bar{0}_x\rangle_1 (\alpha |\bar{0}_y\rangle_2 + i\beta |\bar{1}_y\rangle_2) + |\bar{1}_x\rangle_1 (\beta |\bar{0}_y\rangle_2 + i\alpha |\bar{1}_y\rangle_2). \quad (\text{A5})$$

In App. C we show that Eqn. (A5) is satisfied by U .

Now that the crystal is in the entangled state given in Eqn. (A5), we measure the physical qubits in code 1 in the X basis to teleport the logical information onto code 2. The way we defined the states $|\bar{0}_x\rangle_1$ and $|\bar{1}_x\rangle_1$ implies that, if no dephasing errors occurred, the teleporting X basis measurements will collapse all the qubits to the same Pauli- X eigenstate: either all in the $+1$ or the -1 eigenstate. That is, either all ions will fluoresce or none of them will. However if a few dephasing errors have occurred, the affected qubits will fluoresce differently from the majority. We may then infer the measurement outcome by determining whether the majority of ions fluoresce (the measurement collapsed code 1 to $|\bar{0}_x\rangle_1$) or not (the measured state is $|\bar{1}_x\rangle_1$) [9].

The teleporting measurement supplies us with *syndrome information* of the form ‘most ions fluoresce’ or ‘most ions don’t fluoresce’ which tells us whether we need to apply a correction to code 2 or not. This syndrome information will fail us if more than $(n-1)/2$ of the qubits in code 1 have suffered a dephasing error and the Pauli correction we make after the teleportation will introduce a logical error to code 2.

Finally, it is worth mentioning that we may want to perform this teleporation of logical information between two repetition codes that are supported on partitions of the physical qubits of the system. This will require that

some physical qubits remain disentangled from the encoded logical states. This is possible by preparing the qubits which we wish to remain disentangled in eigenstates of the Pauli- Z operator. Physical qubits prepared in this basis do not entangle with other qubits under the action of U .

3. Encoding onto the repetition code by teleportation

In addition to reading syndrome data to protect logical qubits from errors, we can also prepare arbitrary code-words of the quantum error-correcting code using global operations and single-qubit measurements. If we reconsider the teleportation operation given in the previous Subsection where the first code given in Eqn. (A4), $|\bar{\psi}_y\rangle_1$, only contains a single physical qubit, we see that we can teleport an arbitrary state prepared on a single qubit onto a repetition code.

Appendix B: The centre-of-mass interaction

In this Appendix we show that applying the interaction Hamiltonian given in Eqn. (3) for a time $T = 2\pi k/\delta$ implements the entangling operation U in Eqn. (1). One can check that the global unitary operation U in Eqn. (1) acts like

$$U|\mathbf{s}\rangle = (-1)^{|\mathbf{s}|(|\mathbf{s}|-1)/2} |\mathbf{s}\rangle, \quad (\text{B1})$$

on an arbitrary spin configuration $|\mathbf{s}\rangle = |s_1 s_2 \dots s_N\rangle$ with $s_j = 0, 1$ where $|\mathbf{s}|$ denotes the number of spins in \mathbf{s} that take the value 1. We must show then that we can reproduce the action of U shown in Eqn. (B1) by driving the CoM mode described in Eqn. (3) for a suitable choice of parameters. We consider a system with a spin-dependent ODF [9] whereby ions in the $|0\rangle$ ($|1\rangle$) state experiences a force F_0 (F_1). The entangling operation is least sensitive to laser noise if we set $F_0 = -F_1 = F$, leading to the Hamiltonian defined in Section II A. However other factors may constrain us to unbalanced forces leading to the more general interaction Hamiltonian

$$H_{\text{int}} = \frac{J}{N} \sum_{j < k}^N Z'_j Z'_k, \quad (\text{B2})$$

where

$$Z' = \frac{1}{F} \begin{pmatrix} F_0 & 0 \\ 0 & F_1 \end{pmatrix}, \quad (\text{B3})$$

and $J \approx F^2/4M\omega_1\delta$ with N the number of ions in the crystal, ω_1 the CoM mode frequency, M the ion mass and F the magnitude of the force imparted on individual ions by the travelling one-dimensional optical lattice. For this calculation it will be convenient to write Z' in terms of

Pauli matrices such that $Z'_j = R\mathbb{1}_j + Z_j$ where R captures the imbalance between F_0 and F_1 .

To determine the entangled state we produce we consider the energy eigenvalues of H_{int} . Given that H_{int} is written in terms of Pauli-Z matrices, it is diagonal in the computational basis. Using that $Z'_j |s_j\rangle = (R + 1 - 2s_j) |s_j\rangle$, we satisfy the energy eigenvalue expression $H_{\text{int}} |\mathbf{s}\rangle = \lambda_{\mathbf{s}} |\mathbf{s}\rangle$ with

$$\frac{N\lambda_{\mathbf{s}}}{J} = 4 \sum_{j<k}^N s_j s_k - A \sum_j^N s_j + \text{const.}, \quad (\text{B4})$$

where $A = 2(R + 1)(N - 1)$ and $\text{const.} = N(N - 1)(R + 1)^2/2$, thus giving us the unitary evolution $e^{-iH_{\text{int}}t} |\mathbf{s}\rangle = e^{-i\lambda_{\mathbf{s}}t} |\mathbf{s}\rangle$. We must verify then that we can find system parameters such that

$$e^{-i\lambda_{\mathbf{s}}t} = (-1)^{|\mathbf{s}|(|\mathbf{s}|-1)/2} \quad (\text{B5})$$

for all values of \mathbf{s} . Given that the constant term in Eqn. (B4) introduces an irrelevant global phase to the system, we will consider only the spin-dependent terms.

With a simple calculation we can verify that

$$\sum_{j<k}^N s_j s_k = |\mathbf{s}|(|\mathbf{s}| - 1)/2. \quad (\text{B6})$$

Therefore, if we choose $4Jt/N = \pi$ [23] we have

$$e^{-iH_{\text{int}}t} |\mathbf{s}\rangle = VU |\mathbf{s}\rangle, \quad (\text{B7})$$

up to a global phase, where $V = \exp(iAJt \sum_j s_j/N)$. The effect of V , equivalent to a local Z rotation on every qubit, is to rotate the resultant code states within the logical XY plane, leading to the generalised codewords

$$|\bar{0}_\phi\rangle = \underbrace{|+\phi\rangle |+\phi\rangle \dots |+\phi\rangle}_n, \quad (\text{B8a})$$

$$|\bar{1}_\phi\rangle = \underbrace{|-\phi\rangle |-\phi\rangle \dots |-\phi\rangle}_n, \quad (\text{B8b})$$

where $|\pm\phi\rangle = (|0\rangle \pm e^{i\phi}|1\rangle)/\sqrt{2}$. Such an encoding provides equivalent protection against Z errors, provided we have full knowledge of the angle ϕ , which will define the phase angle of the global microwave pulses used for state readout and preparation. The presence of V is therefore only problematic due to the uncertainty in our ODF, ϵ_F , which leads to an uncertainty in the phase of $\epsilon_\phi = (2\epsilon_F + \epsilon_F^2)$.

Appendix C: Teleporting logical information between two repetition codes

Here we show that the global operation U , as defined in the main text in Eqn. (1), followed by a single-qubit

measurement will teleport logical information from one repetition code to another, up to single-qubit rotations. We will show this statement holds for the case where the two repetition codes have different numbers of qubits, n_1 and n_2 , respectively. It will be convenient to denote the set of all qubits of the system with the label \mathcal{Q} , together with two subsets of qubits which we label \mathcal{Q}_α with $\alpha = 1, 2$ where there is one repetition code written to each of the two qubit subsets.

The controlled-phase gate maps two-qubit states as follows

$$CZ |AB\rangle = (-1)^{AB} |AB\rangle, \quad (\text{C1})$$

where A, B take values 0, 1. In general, we will write the controlled phase gate $CZ_{j,k}$ with indices j, k to specify the control and target qubits which are indexed j and k .

We must show that

$$U |\bar{\Lambda}_A\rangle_1 |\bar{\Lambda}_B\rangle_2 = (-1)^{AB} |\bar{\Lambda}_A\rangle_1 |\bar{\Lambda}_B\rangle_2, \quad (\text{C2})$$

where the states $|\bar{\Lambda}_A\rangle_1$ and $|\bar{\Lambda}_B\rangle_2$ are the basis states for the codewords of the system such that A and B take values 0 and 1 which are defined shortly, and where

$$U = \prod_{\langle j,k \rangle} CZ_{j,k}, \quad (\text{C3})$$

with the product taken over all pairs of qubits in the system.

The codewords of the repetition code we consider are written concisely in the eigenbasis of Pauli-Z matrices such that

$$|\bar{\Lambda}_0\rangle_\alpha = \frac{|\bar{0}_x\rangle_\alpha + |\bar{1}_x\rangle_\alpha}{\sqrt{2}}, \quad |\bar{\Lambda}_1\rangle_\alpha = \frac{|\bar{0}_x\rangle_\alpha - |\bar{1}_x\rangle_\alpha}{\sqrt{2}}, \quad (\text{C4})$$

where $\alpha = 1, 2$ specifies the code written to the qubits of subset \mathcal{Q}_α , and where $|\bar{0}_x\rangle$ and $|\bar{1}_x\rangle$ are defined in Eqns. (A3a) and (A3b). It follows that the codewords written in the computational basis take values

$$|\bar{\Lambda}_0\rangle_\alpha = \sum_{\text{even } |\mathbf{s}|} |\mathbf{s}\rangle_\alpha, \quad |\bar{\Lambda}_1\rangle_\alpha = \sum_{\text{odd } |\mathbf{s}|} |\mathbf{s}\rangle_\alpha, \quad (\text{C5})$$

up to normalisation, where the symbol \mathbf{s} labels bit strings of length n_α and $|\mathbf{s}|$ denotes the number of bits in \mathbf{s} that take the value 1.

We will show Eqn. (C2) holds using the expressions given by Eqns. (C5). To do so, we first consider the action of U on two arbitrary product states of qubits prepared in the computational basis. It is easily checked that

$$U |\mathbf{s}\rangle_1 |\mathbf{t}\rangle_2 = (-1)^{r(r-1)/2} |\mathbf{s}\rangle_1 |\mathbf{t}\rangle_2 \quad (\text{C6})$$

where $r = |\mathbf{s}| + |\mathbf{t}|$ and \mathbf{s} and \mathbf{t} are bit strings of length n_1 and n_2 , respectively. By expanding the exponent $r(r - 1)/2$ in Eqn. (C6) we see that

$$\frac{r(r-1)}{2} = \frac{|\mathbf{s}|(|\mathbf{s}|-1)}{2} + \frac{|\mathbf{t}|(|\mathbf{t}|-1)}{2} + |\mathbf{s}||\mathbf{t}|, \quad (\text{C7})$$

where, importantly, the term $|\mathbf{s}||\mathbf{t}|$ takes an odd value if and only if both $|\mathbf{s}|$ and $|\mathbf{t}|$ are odd. Using this fact, and by expressing codewords in the form given in Eqn. (C5), we see that

$$U |\bar{\Lambda}_A\rangle_1 |\bar{\Lambda}_B\rangle_2 = (-1)^{AB} |\bar{\Lambda}'_A\rangle_1 |\bar{\Lambda}'_B\rangle_2, \quad (\text{C8})$$

such that

$$|\bar{\Lambda}'_0\rangle_\alpha = \sum_{\text{even } |\mathbf{s}|} (-1)^{|\mathbf{s}|(|\mathbf{s}|-1)/2} |\mathbf{s}\rangle_\alpha, \quad (\text{C9})$$

and

$$|\bar{\Lambda}'_1\rangle_\alpha = \sum_{\text{odd } |\mathbf{s}|} (-1)^{|\mathbf{s}|(|\mathbf{s}|-1)/2} |\mathbf{s}\rangle_\alpha. \quad (\text{C10})$$

With some additional analysis of the new states given in Eqns. (C9) and (C10) we see that

$$|\bar{0}_y\rangle = \frac{|\bar{\Lambda}'_0\rangle_\alpha + |\bar{\Lambda}'_1\rangle_\alpha}{\sqrt{2}}, \quad |\bar{1}_y\rangle = \frac{|\bar{\Lambda}'_0\rangle_\alpha - |\bar{\Lambda}'_1\rangle_\alpha}{\sqrt{2}}, \quad (\text{C11})$$

up to an uninteresting global phase. In this basis it is easily seen that we recover the initial code states $|\bar{\Lambda}_0\rangle_\alpha$

and $|\bar{\Lambda}_1\rangle_\alpha$ from the states $|\bar{\Lambda}'_0\rangle_\alpha$ and $|\bar{\Lambda}'_1\rangle_\alpha$ by applying the single qubit rotation $\Gamma_j = (X_j + Y_j)/\sqrt{2}$ on each of the qubits j in qubit subset \mathcal{Q}_α where X_j and Y_j are the standard Pauli-X and Pauli-Y matrices. We thus have that

$$\Gamma U |\bar{\Lambda}_1\rangle |\bar{\Lambda}_B\rangle = (-1)^{AB} |\bar{\Lambda}_A\rangle |\bar{\Lambda}_B\rangle, \quad (\text{C12})$$

as desired, where $\Gamma = \prod_{j \in \mathcal{Q}} \Gamma_j$ which can be inverted using single-qubit rotations, although, from a practical perspective we expect the protocol to be simpler if the physical qubits are left in the rotated basis. Finally, to teleport information encoded on \mathcal{Q}_1 to the second subset, \mathcal{Q}_2 , we must perform a measurement in the logical superposition basis spanned by the vectors shown in Eqn. (C4). This is achieved by measuring one single qubit in the Pauli-X basis. The outcome of this measurement also provides the information we require to determine the correction operator we must apply to the encoded state after the measurement has been made, thus completing the teleportation protocol.

-
- [1] M. D. Reed, L. DiCarlo, S. E. Nigg, L. Sun, L. Frunzio, S. M. Girvin, and R. J. Schoelkopf, *Nature* **482**, 382 (2012).
- [2] R. Barends, J. Kelly, A. Megrant, A. Veitia, D. Sank, E. Jeffrey, T. C. White, J. Mutus, A. G. Fowler, B. Campbell, et al., *Nature* **508**, 500 (2014).
- [3] A. D. Córcoles, E. Magesan, S. J. Srinivasan, A. W. Cross, M. Steffen, J. M. Gambetta, and J. M. Chow, *Nat. Comms.* **6**, 6979 (2015).
- [4] J. Kelly, R. Barends, A. G. Fowler, A. Megrant, E. Jeffrey, T. C. White, D. Sank, J. Y. Mutus, B. Campbell, Y. C. and Z. Chen, et al., *Nature* **519**, 66 (2015).
- [5] M. Takita, A. D. Córcoles, E. Magesan, B. Abdo, M. Brink, A. Cross, J. M. Chow, and J. M. Gambetta, arXiv:1605.01351 (2016).
- [6] J. Chiaverini, D. Leibfried, T. Schaetz, M. D. Barrett, R. B. Blakestad, J. Britton, W. M. Itano, J. D. Jost, E. Knill, C. Langer, et al., *Nature* **432**, 602 (2004).
- [7] D. Nigg, M. Müller, E. A. Martinez, P. Schindler, M. Hennrich, T. Monz, M. A. Martin-Delgado, and R. Blatt, *Science* **345** (2014).
- [8] N. Ofek, A. Petrenko, R. Heeres, P. Reinhold, Z. Leghtas, B. Vlastakis, Y. Lio, L. Frunzio, S. M. Girvin, L. Jiang, et al., arXiv:1602.04768 (2016).
- [9] J. F. Goodwin, B. J. Brown, G. Stutter, H. Dale, R. C. Thompson, and T. Rudolph, *Phys. Rev. A* **92**, 032314 (2015), URL <http://link.aps.org/doi/10.1103/PhysRevA.92.032314>.
- [10] D. P. DiVincenzo and P. W. Shor, *Phys. Rev. Lett.* **77**, 3260 (1996).
- [11] S. D. Barrett and P. Kok, *Phys. Rev. A* **71**, 060310 (2005).
- [12] N. H. Nickerson, Y. Li, and S. C. Benjamin, *Nat. Commun.* **4**, 1756 (2013).
- [13] C. Monroe, R. Raussendorf, A. Ruthven, K. R. Brown, P. Maunz, L.-M. Duan, and J. Kim, *Phys. Rev. A* **89**, 022317 (2014).
- [14] N. H. Nickerson, J. F. Fitzsimons, and S. C. Benjamin, *Phys. Rev. X* **4**, 041041 (2014).
- [15] B. Lekitsch, S. Weidt, A. G. Fowler, K. M. Imer, S. J. Devitt, C. Wunderlich, and W. K. Hensinger, arXiv:1508.00420 (2015).
- [16] K. R. Brown, J. Kim, and C. Monroe, arXiv:1602.02840 (2016).
- [17] P. Webster, S. D. Bartlett, and D. Poulin, *Phys. Rev. A* **92**, 062309 (2015).
- [18] D. Wineland, C. Monroe, W. M. Itano, D. Leibfried, B. E. King, and D. M. Meekhof, *Experimental issues in coherent quantum-state manipulation of trapped atomic ions* (1998).
- [19] B. C. Sawyer, J. W. Britton, A. C. Keith, C.-C. J. Wang, J. K. Freericks, H. Uys, M. J. Biercuk, and J. J. Bollinger, *Phys. Rev. Lett.* **108**, 213003 (2012), URL <http://link.aps.org/doi/10.1103/PhysRevLett.108.213003>.
- [20] D. Leibfried, B. DeMarco, V. Meyer, D. Lucas, M. Barrett, J. Britton, W. M. Itano, B. Jelenkovic, C. Langer, T. Rosenband, et al., *Nature* **422**, 412 (2003).
- [21] R. Ozeri, arxiv:1106.1190v1 (2011).
- [22] T. B. Mitchell, J. J. Bollinger, W. M. Itano, and D. H. E. Dubin, *Phys. Rev. Lett.* **87**, 183001 (2001), URL <http://link.aps.org/doi/10.1103/PhysRevLett.87.183001>.
- [23] In fact, we are free to take $4Jt/N = \pi(1+2l)$ for arbitrary values of l where l is an integer. Ideally, we will choose a value of l that will minimise error.